ISSN NO. 2320-5407

Journal homepage: http://www.journalijar.com

INTERNATIONAL JOURNAL OF ADVANCED RESEARCH

RESEARCH ARTICLE

Fracture Behavior of 6061 Al-Alloy Pipes under Bursting Loads with Crack Length Variation

***D.U.M.Manikanta[1], and A.Chennakesava Reddy[2]**

1. PG Student, Department of Mechanical Engineering, JNTUH College of Engineering, Hyderabad, India.
2. Professor, Department of Mechanical Engineering, JNTUH College of Engineering, Hyderabad, India.

Manuscript Info

Manuscript History:

Received: 11 February 2015
Final Accepted: 22 March 2015
Published Online: April 2015

Key words:
6061, bursting pressure, fracture, crack length, pipes, J-integral, stress intensity factors.

Corresponding Author

D.U.M.Manikanta

Abstract

In this paper 3D finite element analyses were performed to obtain fracture behavior of 6061 Al-alloy pipes subjected to internal bursting pressure. It was observed that the large deformations have promoted the path dependence of the J-integral. It was noticed that the J-integral was dependent on the deformation and the crack area. The values of KI and KII stress intensity factors along the crack-front were very high and, the, mode-I and mode-II were the dominant fracture modes. The pipes were tested till they burst with various crack lengths on them. All the pipes above or below the l/d raio of 90.71 were failed to satisfy yield and ultimate tensile strength criterion.

INTRODUCTION

Metal tubing is used to transfer liquids, air, or solids. Metal tubing is used in heating, ventilation, and air conditioning (HVAC) and plumbing systems and for applications in the aerospace, automotive, chemical processing, food and beverage, manufacturing, and medical industries. 6061 is used for heavy duty structures requiring good strength-to-weight ratio with good corrosion resistance. The most important parameters in designing pipelines are the pressure and temperature of the conveying media. The major concern of pipes is to maintain its geometric integrity to ensure they are safe and effective during operation to avoid unforeseen disaster. One of the major geometric integrity is cracks on the surface (Reddy and Shamraj, 1998). The wall thinning on a pipe due to corrosion, results in localized pit with different depths and lengths on its internal and external surfaces (Hopkins, 2002). The codes such as BS 7910 (1999) and DNV RP-F101 (1999) are the semi-empirical methods used for the assessment of the integrity of pipes. The operating pressure calculation and consequent wall thickness of gas transmission pipelines can be obtained from ASME B31.8 (ASMEB31.8 2012):

$$P = (2\,\sigma t)/D \times F \times E \times T \quad (1)$$

where P is the design pressure (MPa), σ is the specified minimum yield strength (MPa), t is the nominal wall thickness (mm), D is the nominal outside diameter (mm), F is the design factor, E is the longitudinal joint factor and T is the temperature derating factor.

As demonstrated in figure 1, analysis of fracture mechanics is described as three pure modes. In mode one (I) or "opening mode" the displacement of crack surfaces due to normal stresses, is perpendicular to the plane of the crack. In forward shear or mode two (II) or "sliding mode", the displacement of crack surfaces is in the plane of the crack and normal to the crack front line. The "tearing mode" or mode three (III) is caused by anti plane shear and the crack surface displacements are parallel to the crack front line and in the plane of the crack. The stress intensity factor (SIF) represented by capital K. The K subscripts I, II and III stands for different loading conditions.

In a pure elastic crack, stress singularity at the crack tip is dominant. Due to the yield stress of materials

especially in metals, for stresses above the young's modulus (σ_y) the material deforms plastically. So stress singularity cannot exist. Figure 2 illustrates an approximate stress distribution at the crack tip with a plastic zone. The crack tip plasticity causes lower stiffness and larger displacements than in the elastic case (Irwin, 1957). Similar to linear elastic cases, an energy release rate for nonlinear elastic bodies can be defined as the area on the load displacement diagram between crack areas A and A+dA, as shown in figure 3. The nonlinear energy release rate *J*, for constant load and constant displacement has been defined as:

$$J = \left|\frac{\partial \pi}{\partial A}\right| \quad (2)$$

The finite element analysis (FEA) is one of the most efficient tools to quantify reliably the remaining strength of corroded pipes. Elastic-plastic finite element models have been used to provide more accurate results in evaluating the corrosion defects (Cosham et al., 2007). ANSYS (2010) can be used to numerically evaluate the collapse pressure of crack defects. When a corrosion/flaw defect occurs on the internal or external pipe surface, the integrity of the pipe is reduced. The important parameters that determine the strength of a pipe are as follows (Stephens, 1997):

- Internal pressure
- Pipe Diameter
- Crack depth related to the wall thickness
- Crack length related to the pipe length
- Stress distribution
- Total deformation
- J-integral
- Stress intensity factors (SIFs): KI, KII and KIII

The present work is aimed at to study the finite element analysis of crack propagation and pipe bursting with predefined flaws of varying length and depth. The pipes are analyzed for various bursting pressures. As illustrated in figure 4, the longitudinal crack length is shown at '2*a'* and the pipe is under an internal pressure loading of '*p'*, with the pipe thickness depicted as' *t*'.

Material and Methods

Experiments were performed on 6061 Al alloy pipes. Eight types of 6061 Al-alloy tubes of different crack lengths as shown table 1 for the same outer diameter (41.28 mm) were used for experimentation. A surface notch as shown in figure 4 made on the outer surface of the specimen was used as a preflaw for experimentation. Outer surface notches provide an indication of system response to discontinuities originating from the outer surface. The dimensions of notches are given in table 1. Outer surface notches were produced in the middle of the tube length by electric discharge machining (EDM). The specimens were coded as shown in table 1 for easy monitoring during experimentation.

High pressure testing machine (2000 bar) as shown in figure 5 was used for hydrostatically testing of 6061 Al-alloy pipes. The tube specimen was fixed to the main pressure hose of the testing unit with a threaded plug as shown in figure 6. On running motor of the pump the pressure was gradually developed, on increasing the pressure further gradually, the specimen was started yielding at the notch. When the pressure was still increased the specimen was burst at the notch. The specimen code and the corresponding pressure were recorded for each specimen.

Finite Element Modeling

The cross-section of the pipe was created in 2-D and then it was extruded for the given pipe length along the z-direction (Chennakesava, 2008). The ANSYS code was used to model the pipe and initial semi-elliptical crack. The pipe was modeled with tetrahedron elements. The crack and pipe dimensions are given in table-1. The crack geometry is shown in figure 4. Fracture module method for crack generation required that elements must be of higher order. Therefore, the tetrahedral elements of type SOLID 186 were chosen for accurate results (Chennakesava, 2009., Jyothirmai et al., 2005., Reddy, 2006). Fine mesh was used to model the crack region. The number of elements for the tube lengths of 914 mm and 610 mm were 1,74,512 and 1,17,543 respectively. A three-dimensional semi-elliptical crack was initiated on the pipe surface. The crack was oriented with respect to pipe axis. In order to create the semi-elliptical crack onto to the surface, a local coordinate system was established. With reference to the local co-ordinate system and the crack was created on the outer surface of the pipe as shown in figure 7. The pressure was applied on the pipe's inner surface.

Stress intensity is defined as the largest of the absolute values of σ_1 - σ_2, σ_2 - σ_3, or σ_3 - σ_1 (Neewman and Raju, 1981):

$$\sigma_I = MAX\left(|\sigma_1 - \sigma_2|, |\sigma_2 - \sigma_3|, |\sigma_3 - \sigma_1|\right) \quad (3)$$

Stress intensity is related to the maximum shear stress:

$$\sigma_I = 2\tau_{max} \quad (4)$$

Elastic strain intensity is defined as the largest of the absolute values of ε_1 - ε_2, ε_2 - ε_3, or $\varepsilon 3$ - $\varepsilon 1$:

$$\varepsilon_I = MAX\left(|\varepsilon_1 - \varepsilon_2|, |\varepsilon_2 - \varepsilon_3|, |\varepsilon_3 - \varepsilon_1|\right) \quad (5)$$

Elastic strain intensity is equal to the maximum shear elastic strain:

$$\varepsilon_I = \gamma_{max} \quad (6)$$

The maximum equivalent stress safety tool is based on the maximum equivalent stress failure theory for ductile materials, also referred to as the von Mises-Hencky theory. The discretized form of the J-Integral is given by:

$$J = \sum_{ie=1}^{ne}\left[\sigma_{ij}\frac{\partial u_j}{\partial x_1} - w\,\delta_{1i}\right]\frac{\partial q}{\partial x_i} w_{iw} A_{ie} \quad (7)$$

where n_e is the number of elements to be integrated, w_{iw} is the weight function, and A_{ie} is the area of the element represented by ie.

For higher-order elements (such as SOLID186), the q vector at mid-side nodes takes the averaged values from the corresponding corner nodes. For a 3-D problem, domain integral representation of the J-Integral becomes a volume integration, which again is evaluated over a group of elements. The implementation becomes more complicated; however, the principal is similar to the 2-D problem. The near-crack-tip behavior of stress is usually thought to be that of plane strain. K_I, K_{II}, K_{III} were obtained from KCALC command.

Results and Discussion

The results from the finite element software ANSYS were verified with a few critical results through experimentation.

Static Deformation

Table 2 gives the total deformation values of the tested pipes with different crack geometry and bursting pressure. The effect of pipe length /crack depth (l/d) ratio on the total deformation is plotted in figure 8. The l/d ratio of 6.75 for test coupon 4 of 107.14 for test coupon 7 gave the maximum total deformation of 7.6145×10^{-2} mm and 7.6786×10^{-2} mm respectively along the crack depth direction. In both the cases the bursting pressure was 6.1 MPa. The least total deformation was with test coupon 6 of l/d (= 90.71) ratio. The experimental fractures are compared with fracture results obtained from FEA for the test coupons 4, 6 and 7 in figure 9. The FEA results were in good agreement with experimental values.

Stress Distribution across the Crack

The equivalent stress distribution across the crack for all the test coupons is shown in figure 10. The maximum equivalent stress of test coupons 1, 2, 3, 4, 5, 6, 7 and 8 were found to be 703.24 MPa, 672.18 MPa, 616.11 MPa, 664.08 MPa, 528.19 MPa. 339.21 MPa, 616.97 MPa and 671.76 MPa respectively.

If the failure is defined by material yielding, it follows that the design goal is to limit the maximum equivalent stress to be less than the yield strength of the material:

$$\frac{\sigma_e}{S_y} < 1 \quad (8)$$

An alternate but less common definition states that fracturing occurs when the maximum equivalent stress reaches or exceeds the ultimate strength of the material:

$$\frac{\sigma_e}{S_u} < 1 \quad (9)$$

The yield strength and tensile strength of 6061 Al alloy are 276 MPa and 310 Mpa respectively. The ratio of σ_e/σ_y and σ_e/σ_{ts} are plotted for all the test coupons in figure 11a. The test coupons 1, 3, 4, 7 and 8 were burst at pressure 6.1 MPa, while the test coupon 5 was burst at 5.1 MPa and the test coupons 2 and 6 were burst at 4.0 MPa. In all the cases the pressure was extended till they burst (experimentally). Under the same pressure the pipes were analyzed using FEA software. The FEA results were in total agreement with the experimental results. The test

coupon 6 was observed to be at the threshold of safe limit under the criteria based on the ultimate tensile strength. However, all the test coupons were not satisfying the criteria based on the yield strength.

The FEA procedure was repeated for all the test coupons with safe pressure (3.5 MPa) lesser than that (4.0 MPa) was observed with test coupon 6. The failure criterion are plotted as shown in figure 11b. Both the criterion of yield strength and ultimate tensile strength was satisfied with l/d ratio of 90.71. All the pipes above or below the l/d raio of 90.71 were failed to satisfy any one of the criteria.

J-Integral

The J-integral is equal to the strain energy release rate for a crack in a body subjected to monotonic loading. The path dependence of the J-integral is displayed for all ten specimens are shown in figure 13(a). For a crack in an elastic body subject to a load, the elastic energy stored in the body is a function of two independent variables: the displacement of the load, and the area of the crack. The total displacement of the test coupons 4, 6 and 7 were respectively 7.62mm, 4.92mm and 7.68 mm. The crack area for the test coupons 4, 6 and 7 were nearly 21.17 mm^2, 33.60 mm^2 and 33.60 mm^2 respectively. The maximum values of J-integrals 0.985MJ-mm^2, 0.329MJ-mm^2 and 0.591MJ-mm^2 of the test coupons 4, 6, 7 were arrived at distances of 49.82mm, 49.82mm and 106.76mm respectively. The path dependence of the J-integral was much more significant in a large deformation analysis (Reddy et al., 2005). The far field value of J was reached with test coupon 7 latter, whereas in the test coupon 6 having small deformation the far field value of J was already reached. However, the far field value of J for the test coupon 4 had reached at the distance of the test coupon 6, the total deformation and J-integral value of the test coupon 4 were much higher than the test coupon 6. The shear stress values of the test coupon 4, 6 and 7 are 369.34 MPa, 171.29 MPa and 234.77 MPa respectively.

Stress Intensity Factors

Each test coupon was started with a pre-existing crack of a given length "2a". Mode I was a spreading apart of the two halves of the crack interface, recognizable as the most severe case. The stress intensity factor (K) is a defined as the product applied macroscale stress (σ), the square root of the crack length (2a), and a constant that depends on the particular fracture mode and geometry of the test specimen. The stress intensity factor for Mode I is designated KI, KII for Mode II, and KIII for Mode III.

Figure 13 shows the variations of stress intensity factors (KI, KII, and KIII) along the initial crack-front. Figures 13(d) indicates that the values of KIII stress intensity factors along the crack-front were very small. KII was higher than KIII also (figure 13(c)). Therefore, mode-I and mode-II were the dominant fracture modes. Figure 13(b) shows that the mode-I stress intensity factors at the crack-front of all the pipes. The pipe 6 was reported to have the minimum values of KI and KII. All stress intensity factors were increased with enlarging the crack length.

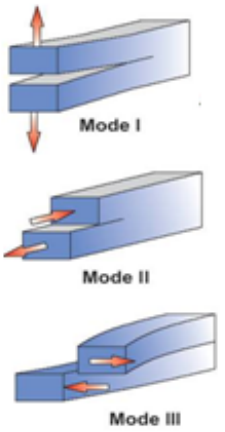

Figure 1:Modes of crack

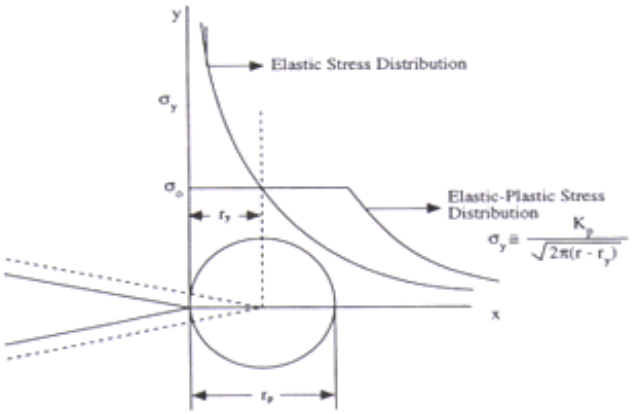

Figure 2. Elastic and Elastic-Plastic crack tip stress distribution in front of the crack tip and the plastic zone sized r_Y and r_p

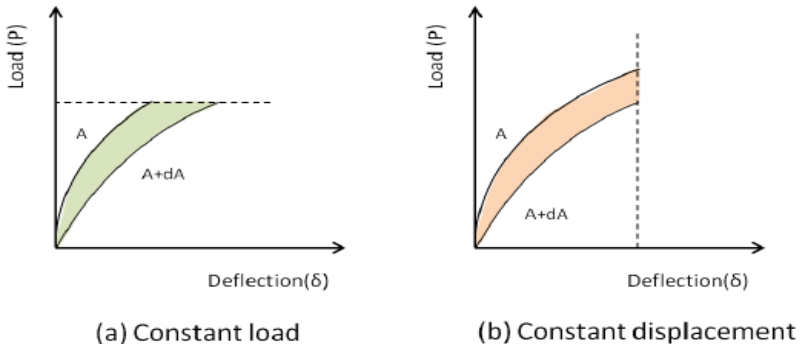

Fig. 3. Available energy for crack extension in a non linear elastic material under different conditions.

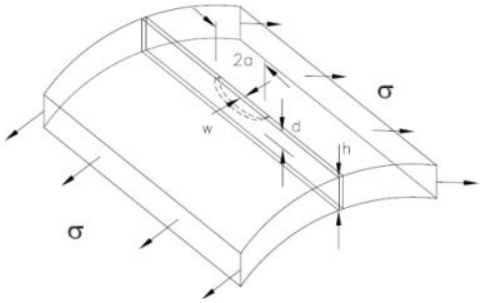

Fig. 4. Crack dimensions.

Fig. 5. High pressure testing machine of pipes

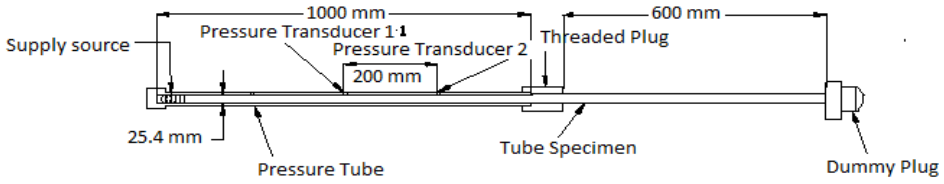

Fig. 6. Tube assembly for high pressure hydrostatic testing of tube specimen.

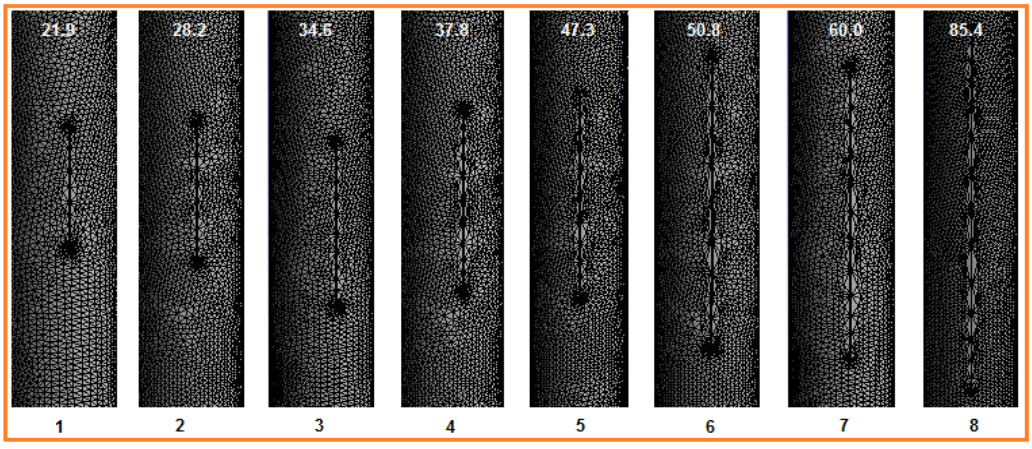

Fig. 7. Mesh view of crack on the pipe surface.

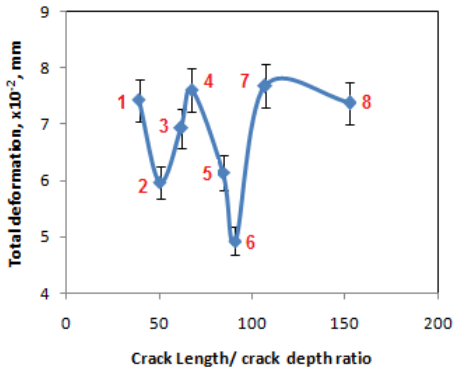

Fig. 8. Total deformation along crack length

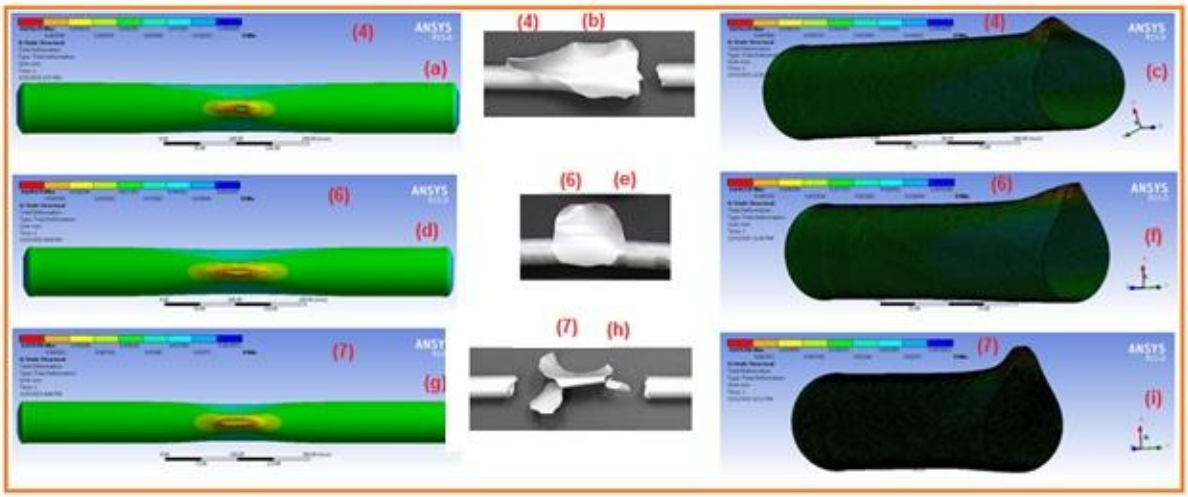

Figure 9: Total deformation of test coupon 4: (a) full pipe (b) experimental, and (c) sectional view of pipe, of test coupon 6: (d) full pipe (e) experimental, and (f) sectional view of pipe and of test coupon 7: (g) full pipe (h) experimental, and (i) sectional view of pipe

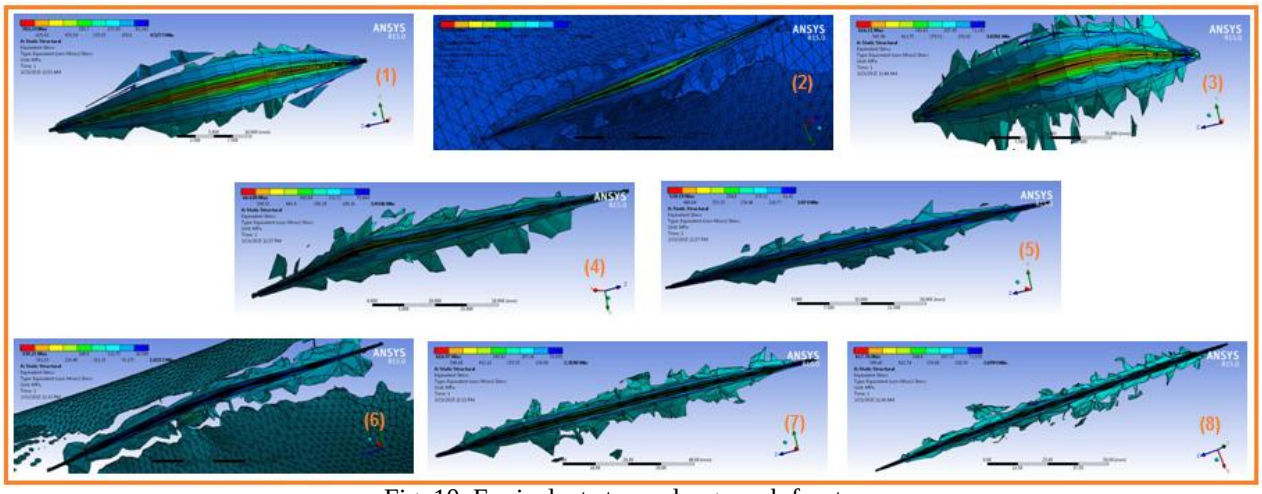

Fig. 10. Equivalent stress along crack front.

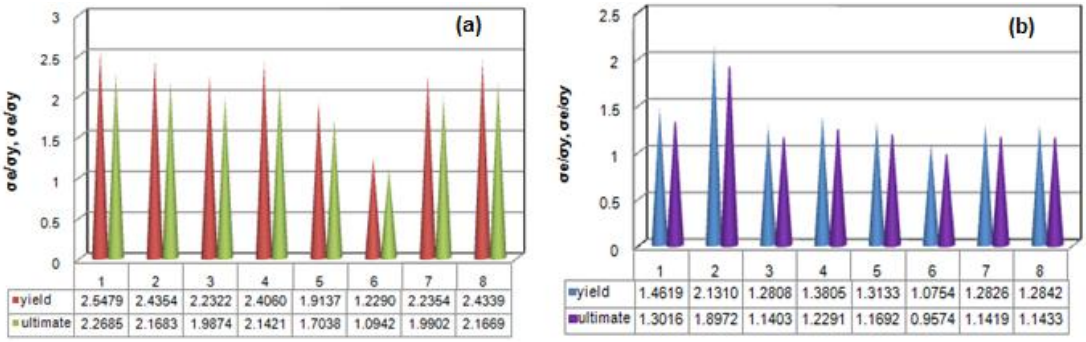

Fig. 11. Failure criteria based on yield and tensile strengths: based on different bursting pressures and (b) based on same bursting pressure

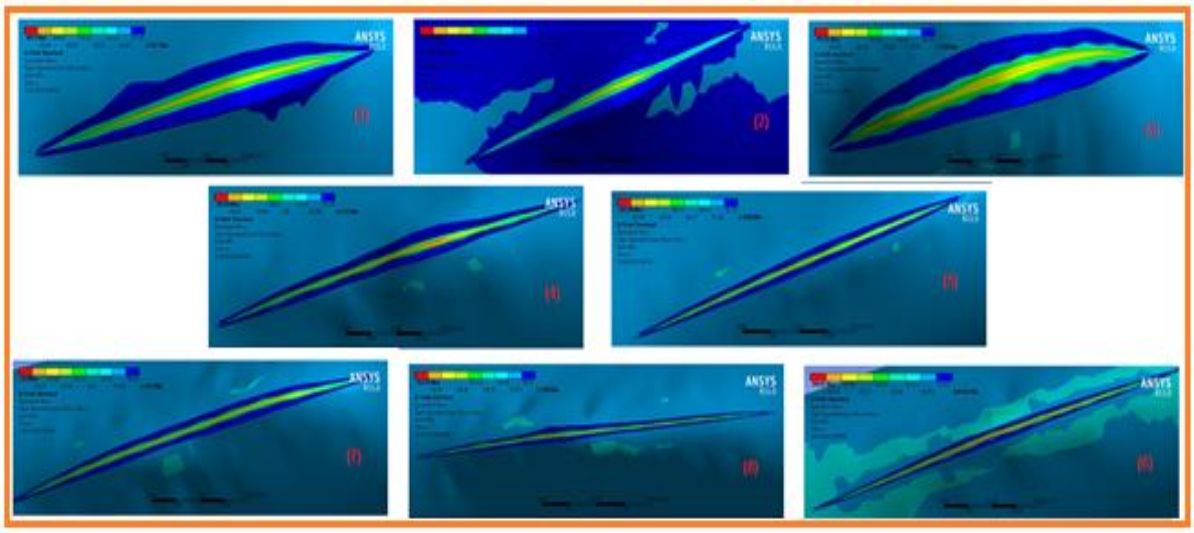

Fig. 10. Equivalent stress along crack front subject to bursting pressure of 3.5 MPa.

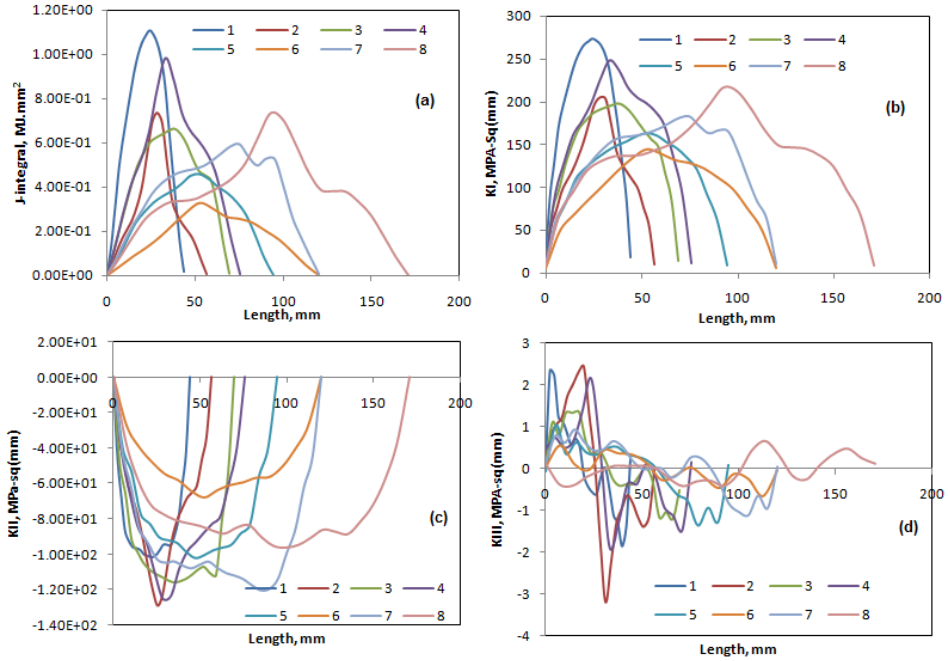

Figure 11: J-integral (a),stress intensity factor KI (b),stress intensity factor KII (c) and stress intensity factor KIII(d)

TABLE 1: Testing Conditions of Pipes

Test coupon	Diameter of pipe, D (mm)	Thickness of pipe, t (mm)	Length of pipe, L (mm)	Crack length (2a)	Crack width, w (mm)	Crack depth, d (mm)	Pressure, MPa
1	41.28	0.89	914	21.9	0.2	0.56	6.1
2	41.28	0.89	610	28.2	0.2	0.56	4.0
3	41.28	0.89	914	34.6	0.2	0.56	6.1
4	41.28	0.89	610	37.8	0.2	0.56	6.1
5	41.28	0.89	610	47.3	0.2	0.56	5.1
6	41.28	0.89	610	50.8	0.2	0.56	4.0
7	41.28	0.89	914	60.0	0.2	0.56	6.1
8	41.28	0.89	914	85.4	0.2	0.56	6.1

TABLE 2: Deformation Results of Pipes

Test coupon	Total deformation, mm x e-02
1	7.4348
2	5.9673
3	6.9276
4	7.6145
5	6.144
6	4.9235
7	7.6786
8	7.3768

Conclusions

In this paper 3D finite element analyses considering a general mixed-mode fracture condition were performed to obtain the crack growth behavior of 6061 Al-alloy pipes subjected to internal bursting pressure. It was observed that the path dependence of the J-integral was much more significant in a large deformation analysis. The values of KI and KII stress intensity factors along the crack-front were very high. All the pipes above or below the l/d raio of 90.71 were failed to satisfy yield and ultimate tensile strength criterion.

Acknowledgements

The authors thank the University Grants Commission (UGC) – New Delhi for assisting financially this project under PG project assistantship from SAP-UGC project sanctioned to the Department of Mechanical Engineering, JNT University Hyderabad.

References

ANSYS Inc. ((2010): www.ansys.com.

BS7910 (1999): Guide on Methods for Assessing the Acceptability of Flaws in Metallic Structures- Annex G: The Assessment of Corrosion in Pipes and Pressure Vessels, British Standard.

Chennakesava, R. A. (2008): CAD/CAM: Concepts and Applications, PHI Learning Pvt. Ltd.

Chennakesava R. A. (2009): FEM: Basic Concepts and Applications, PHI Learning Pvt. Ltd.

Cosham, A., and Hopkins, P. (2007): Best Practice for the Assessment of Defects in Pipelines-Corrosion, Engineering Failure Analysis, 1245-1265.

DNV, Recommended Practice DNV RP-F101 (1999): Corroded Pipelines, Det Norske Veritas, Norway.

Hopkins, P. (2002): Training Engineers in Pipeline Integrity, Western Regional Gas Conference, Arizona, EUA.

Irwin, G.R. (1957): Analysis of stresses and strains near the end of a crack traversing a plate, Applied Mechanics, 24:361–364.

Jyothirmayi, N., and Reddy, A.C., and Balu Naik B. (2005): Finite element analysis of Ti-alloy fracture behavior and experimental validation, National Conference on Advances in Mechanical Engineering, Hyderabad.

Newman, Jr. J.,and Raju, I. S. (1981): An Empirical Stress-Intensity Factor Equation for the Surface Crack, Engineering Fracture Mechanics, 15:185–192.

Reddy, A. C. (2006): Finite element analysis of reverse superplastic blow forming of Ti-Al-4V alloy for optimized control of thickness variation using ABAQUS, Journal of Manufacturing Engineering, 1(1):6-9.

Reddy, A.C., Reddy, P. R., and Kotiveerachari, B. (2005): Large rotation and large deformation analysis of four-bar mechanism, National Level Technical Symposium Nalgonda, India.

Reddy, A.C., and Shamraj, V.M. (1998): Reduction of cracks in the cylinder liners choosing right process variables by Taguchi method, Foundry Journal, 10 (4):47-50

Stephens, D. R., Leis, B. N., and Rudland, D. L. (1997): Influence of Mechanical Properties and Irregular Geometry on Pipeline Corrosion Defect Behavior.